Obtaining Surface Curvature and Depth Information With a Disparity-Based Photometric Stereo

José R. A. Torreão
Cecilio J. L. Pimentel
Edward Roe

Departamento de Informática, Universidade Federal de Pernambuco
50.732-970 Recife, PE, Brasil

Abstract. Disparity-Based Photometric Stereo (DBPS) is a recently introduced Computer Vision process which extracts a disparity field from two or more photometric stereo images by tracking the displacement of pixel intensities resulting from the change in the illumination of the observed scene. Such photometric-disparity field is akin to the disparity field due to the change of viewing position in Stereoscopy, and can be obtained through essentially the same stereo correspondence algorithms. In the present article, we relate the photometric-disparity field to the curvature of the imaged surfaces, and also show how it can be used for the inference of depth through a new version of the Dual Photometric Stereo process, which employs two cameras and multiple illuminations. We illustrate our approach with a neural net simulation of the stereo correspondence algorithms.

Introduction

Stereoscopy and Photometric Stereo are two processes which are widely used for the estimation of geometric properties of imaged surfaces in Computational Vision. The first, also known as Geometric Stereo [**Grimson 86, Barnard 82**], extracts depth information from the displacement of features (which is called 'disparity') observed when two images of a scene are captured from different viewing positions. At the core of that process is the matching of points in the two images which are projections of the same location in the scene. Photometric Stereo [**Woodham 80**], on the other hand, is a Reflectance Map technique employing two or more images, obtained from a single camera for different illumination directions, which allows the estimation of an orientation map for the viewed surfaces. The relevant information, in this case, is yielded by the multiple intensity values at each pixel site.

Disparity-Based Photometric Stereo (DBPS) is a recently introduced process [**Torreão 92**] which incorporates aspects of both Stereoscopy and Photometric Stereo. It is based on the fact that, for smooth surfaces, a change in the illumination direction entails a displacement of intensities in the image lattice which can yield a disparity field akin to the one resulting from the change of viewing position in Stereoscopy. Thus, in DBPS, the photometric stereo images are matched to produce a photometric-disparity field which carries information about the curvature of the pictured surfaces, as shown in the next section.

The matching of the photometric stereo images can be accomplished via any appropriate stereo correspondence algorithm. In a previous publication [**Torreão 93**], we reported results obtained with the implementation of DBPS through the stochastic matching algorithm suggested in [**Barnard 86**]. Here, we present further results obtained with a neural network simulation of the matching algorithm, as proposed by Zhou and Chellappa in [**Zhou 88**], and we also illustrate the use of DBPS for the recovery of absolute depth information through a new rendition of the Dual Photometric Stereo process proposed in [**Ikeuchi 87**]. In Ikeuchi's method, two pairs of photometric stereo images obtained from cameras in different locations are used for producing two orientation maps (needle maps) of the imaged surfaces, via the traditional Photometric Stereo process. The orientation maps are then stereoscopically matched and the resulting disparity field yields the desired depth information. In our version of the Dual Photometric Stereo, instead of the needle maps, we match the photometric-disparity fields obtained from DBPS. Our method then retains the desirable feature of allowing the inference of depth from the matching of surface attributes (as opposed to the matching of image data), while presenting the added advantage of permitting the whole process to be based on a single matching algorithm, since both the extraction of the photometric-disparity fields through DBPS, and the

matching of such fields in stereoscopy require just one and the same algorithm.

In the next section, we show how surface curvature can be obtained by the photometric matching in DBPS; following that, we present our experimental results, and conclude with some remarks in the last section.

Surface Curvature and DBPS

Let us consider a pair of photometric stereo images, I_1 and I_2. It is known that the image intensities can be related to the reflectance map function [**Horn 77**] via the image irradiance equations

$$\begin{cases} I_1(x,y) = R_1(p_s, q_s) \\ I_2(x,y) = R_2(p_s, q_s), \end{cases} \tag{1}$$

where $p_s = \left(\frac{\partial z}{\partial x}\right)_s$ and $q_s = \left(\frac{\partial z}{\partial y}\right)_s$ are the gradient components of the imaged surface $z(x,y)$ at the point $s = (x,y)$ (we assume an orthographic imaging projection, such that the X and Y axes of the images coincide with the X and Y axes of the scene), and where the reflectance map functions R_1 and R_2 correspond to the two different illumination directions employed, $\hat{S}_1$ and $\hat{S}_2$, i.e.,

$$R_i(p_s, q_s) \equiv R(p_s, q_s; \hat{S}_i), \quad i = 1, 2. \tag{2}$$

In the traditional Photometric Stereo process [**Woodham 80**], the pair of equations in (1) are solved for the gradient components p_s and q_s. In DBPS, on the other hand, the two images are matched to produce a photometric-disparity map, $\{D(s) = (D_X(s), D_Y(s))\}$, for which the absolute difference

$$|I_1(s) - I_2(s + D(s))| \tag{3}$$

is minimized at every point $s = (x,y)$ in the image lattice. In [**Torreão 92**], this has been done through the use of the stereo matching algorithm proposed by Barnard in [**Barnard 86**], which employs Simulated Annealing [**Kirkpatrick 83**] for minimizing a cost function incorporating the term in (3) and an additional smoothness measure for $\{D(s)\}$.

Instead of dealing with the general form of the disparities, we usually restrict ourselves to those along the X or Y directions on the image plane, which corresponds – in terms of the parallel between DBPS and Stereoscopy [**Torreão 92**] – to considering a horizontal or vertical epipolar geometry. When matching the photometric stereo images along horizontal lines, for instance, we can relate the resulting disparity field to the curvature of the imaged surface along the X direction, as follows:

The matched intensities on the second image, $I_2(x + D_X(s), y)$, can be expressed as

$$I_2(x + D_X(s), y) = R_2(p_{s'}, q_{s'}) \approx R_2(p_s, q_s) + \\ + D_X(s)\left[\left(\frac{\partial R_2}{\partial p}\right)_s \left(\frac{\partial p}{\partial x}\right)_s + \left(\frac{\partial R_2}{\partial q}\right)_s \left(\frac{\partial q}{\partial x}\right)_s\right], \tag{4}$$

where $s = (x,y)$, as before, and where $s' = (x + D_X(s), y)$ is the point in I_2 which has been matched to point s in I_1. Equation (4) will give a good approximation to $I_2(s')$ for slowly curving surfaces, where $\left(\frac{\partial p}{\partial x}\right)$ and $\left(\frac{\partial q}{\partial x}\right)$ are small.

Now, using equation (1), and recalling that the DBPS matching minimizes the difference in equation (3), we can rewrite (4) as

$$I_1(s) \approx I_2(s) + \\ + D_X(s)\left[\left(\frac{\partial R_2}{\partial p}\right)_s \left(\frac{\partial p}{\partial x}\right)_s + \left(\frac{\partial R_2}{\partial q}\right)_s \left(\frac{\partial q}{\partial x}\right)_s\right].$$

Thus, for every point on the image lattice, we have

$$\left(\frac{\partial R_2}{\partial p}\right)\left(\frac{\partial p}{\partial x}\right) + \left(\frac{\partial R_2}{\partial q}\right)\left(\frac{\partial q}{\partial x}\right) \approx \frac{\Delta I}{D_X}, \tag{5}$$

where $\Delta I = I_1(s) - I_2(s)$, and where we omit the dependences on s, for simplicity.

Repeating the above for a DBPS matching along the Y direction, we obtain

$$\left(\frac{\partial R_2}{\partial p}\right)\left(\frac{\partial p}{\partial y}\right) + \left(\frac{\partial R_2}{\partial q}\right)\left(\frac{\partial q}{\partial y}\right) \approx \frac{\Delta I}{D_Y}, \tag{6}$$

which, along with (5), gives us two equations for the curvature components $\left(\frac{\partial p}{\partial x}\right)$, $\left(\frac{\partial p}{\partial y}\right)$, $\left(\frac{\partial q}{\partial x}\right)$ and $\left(\frac{\partial q}{\partial y}\right)$.

Now, if we repeat the foregoing development with a third photometric stereo image, $I_3(x,y) = R_3(p_s, q_s)$, we can further get the equations

$$\left(\frac{\partial R_3}{\partial p}\right)\left(\frac{\partial p}{\partial x}\right) + \left(\frac{\partial R_3}{\partial q}\right)\left(\frac{\partial q}{\partial x}\right) \approx \frac{\Delta I'}{D'_X}, \tag{7}$$

and

$$\left(\frac{\partial R_3}{\partial p}\right)\left(\frac{\partial p}{\partial y}\right) + \left(\frac{\partial R_3}{\partial q}\right)\left(\frac{\partial q}{\partial y}\right) \approx \frac{\Delta I'}{D'_Y}, \tag{8}$$

with $\Delta I' = I_1(s) - I_3(s)$, and where D'_X and D'_Y are the photometric disparities along the X and Y directions, respectively, obtained from images I_1 and I_3.

Equations (5) to (8) can be expressed in matrix form as

$$\mathbf{H} = \begin{pmatrix} \frac{\Delta I}{D_X} & \frac{\Delta I'}{D'_X} \\ \frac{\Delta I}{D_Y} & \frac{\Delta I'}{D'_Y} \end{pmatrix} \begin{pmatrix} R_{2p} & R_{3p} \\ R_{2q} & R_{3q} \end{pmatrix}^{-1}, \quad (9)$$

where the matrix $\mathbf{H} = \begin{pmatrix} p_x & q_x \\ p_y & q_y \end{pmatrix}$ is called the Hessian matrix of $z(x, y)$ (We are using the subscripts x, y, p, and q to denote differentiation with respect to those variables). For smooth surfaces, the integrability condition $p_y = q_x$ holds, and the Hessian is a symmetric matrix.

From the Hessian and the gradient (p, q) of the surface (which can be recovered by the standard photometric stereo process [**Woodham 80**]), intrinsic object-centered representations of surface curvature can be constructed, given for instance in terms of the Gaussian (K) and mean (H) curvatures, which are related to the principal curvatures k_1 and k_2 as $K = k_1.k_2$ and $H = (k_1 + k_2)/2$. The relationship between the Gaussian curvature and the Hessian, for example, is given by

$$K = \frac{\det \mathbf{H}}{(1 + p^2 + q^2)^2}, \quad (10)$$

and thus the sign of the Hessian determinant gives the sign of the Gaussian curvature. This is a useful relation, since the sign of the Gaussian curvature allows the classification of the surface as elliptic (if $K > 0$), hyperbolic (if $K < 0$) or parabolic (if $K = 0$). For some limited purposes, this kind of qualitative structural information about the imaged objects may be sufficient, and a complete map of the shape parameters may not be necessary. In the following section, we describe some preliminary experiments based on such approach.

Experimental Results

We present three experiments illustrating the extraction of shape and depth information from photometric stereo images, through the DBPS process. In the first experiment, we show how cylindrical surfaces can be correctly classified as such by performing the analysis described in the previous section for two pairs of photometric stereo images. The second experiment deals with the estimation of depth via a Dual Photometric Stereo implementation based on the disparity maps yielded by DBPS. There, we match the disparity fields obtained from two pairs of photometric stereo images, where each pair is captured from a different camera, in a stereoscopic arrangement. Finally, in the third experiment, we illustrate how, even from a single pair of images, interesting information about the scene can be inferred from DBPS: the scene can, for instance, be easily segmented into curved and flat regions, and the local concavity or convexity of the surface along the X and Y directions can be established from the sign of the disparities D_X and D_Y.

In all the experiments described, the photometric disparity maps have been obtained through the use of a matching algorithm based on the digital neural network suggested for stereoscopic correspondence in [**Zhou 88**]. Such network consists of $N \times N \times D$ neurons – with $N \times N$ being the size of the image, and D being the maximum disparity value assumed –, where the state of each neuron is $v_{i,j,k} \in \{0, 1\}$, with $v_{i,j,k} = 1$ meaning that the value of disparity at site (i, j) in the image lattice is k.

The synaptic weights between neurons, and the biases are given respectively by

$$T_{i,j,k;l,m,n} = -48\lambda\delta_{i,l}\delta_{j,m}\delta_{k,n} + 2\lambda \sum_{s \in S} \delta_{i,l}\delta_{j,m\oplus s}\delta_{k,n}$$

and

$$I_{i,j,k} = -(I_1(i, j) - I_2(i, j \oplus k))^2,$$

where $f_{a\oplus b} = f_{a+b}$, if $0 \leq a + b \leq N$, and zero, otherwise, and where S is an index set for all neighbors in a 5×5 window centered at point (i, j).

The energy of such network (which is minimized in its steady state) is given by

$$E = \sum_{i=1}^{N}\sum_{j=1}^{N}\sum_{k=0}^{D}(I_1(i, j) - I_2(i, j \oplus k))^2 v_{i,j,k} +$$

$$+\frac{\lambda}{2}\sum_{i=1}^{N}\sum_{j=1}^{N}\sum_{k=0}^{N}\sum_{s \in S}(v_{i,j,k} - v_{i,j\oplus s,k})^2,$$

where λ is a free parameter.

Experiment 1:

In Figures 1a to 1c, we show three photometric stereo images of a scene containing two cylindrical plastic bottles, one horizontal and the other vertical. The image on top (which corresponds to I_1 in equation (1)) was obtained with central illumination, while the other two (images I_2 and I_3) were taken for illumination directions approximately on the ZX and ZY planes, respectively. The resulting photometric-disparity maps D_X and D'_Y are shown in Figures 1d and 1e (we omit the other two maps, D'_X and D_Y, for simplicity). We observe the expected characteristics of those maps: the regions of the

scene that do not curve along the X direction disappear in D_X (black areas), while the same is true for the regions that are flat along Y, in D'_Y. This information, along with similar results derived form D'_X and D_Y, leads immediately, via equations (9) and (10), to the conclusion that the imaged surfaces are cylinders (Gaussian curvature $K = 0$). Furthermore, information about the spatial attitude and the convexity of the two cylindrical areas – which have been clearly segmented in the images – can also be derived from an analysis of the local values (and signs) of the disparities along the X and Y directions. (In the cylindrical patches, higher curvatures are coded as lower gray-level values).

Experiment 2:

Figures 2a and 2b show two photometric stereo images from which the horizontal disparity map (D_X) in Figure 2c was obtained. For the same scene, observed from a different position, the images in Figures 2d and 2e were taken, with the corresponding photometric horizontal disparity map presented in Figure 2f. Now, matching such map to the one in Figure 2c, the stereoscopic disparities in Figure 2g resulted.. There, we have higher gray-levels coding higher disparities, and thus, points in the scene that are closer to the observer. It is then evident that the different depths corresponding to each of the bottles and to the scene background have been clearly discriminated in the process. As we have already mentioned, for the inference of depth, the matching of the photometric disparities should be preferable over the direct matching of image intensities, since the first encode explicit shape properties, while in the latter such properties are still masked by the imaging process.

Experiment 3:

Here we deal with an obviously nontrivial surface: a woman's face. Shown are the two input images (Figures 3a and 3b) and the resulting disparity map D_X (Figure 3c) (here, we employ only one pair of photometric stereo images). In Figure 3b, zero curvature is coded as black (which corresponds to the scene background); gray-levels higher than 7 represent concave regions (with curvature increasing for higher gray-levels), and those lower than 7 represent convex regions (with curvature increasing for lower gray-levels).

The results obtained agree remarkably well with the qualitative shape features of a face: there are mostly convex regions, with the curvature along the X direction increasing (darker areas) as we move along the cheeks towards the edges. Also, the concave intensity peaks (brightest areas) in Figure 3b mark the positions of the lips, eyes, and nose, around which a change in the sign of the curvature along the X direction is indeed to be expected.

This example is illustrative of the potential of DBPS for the inference of useful qualitative shape information, even from images obtained under loosely controlled conditions, in the presence of shadows and other artifacts, and with little – if any – knowledge about the reflectance map of the surfaces. This is in contrast to the known restrictions that apply to the traditional photometric stereo process [**Woodham 80**].

Concluding Remarks

We have shown that the Disparity-Based Photometric Stereo process can be used for the construction of a complete curvature map of the imaged surfaces, with potential applications to the invariant representation and recognition of shapes in Computational Vision. Even when such a complete shape map is not sought, DBPS can yield important qualitative features of the surfaces, which can be used, for instance, in their classification.

We have also considered the use of the photometric disparity maps as inputs for stereoscopic matching: With two pairs of photometric stereo images obtained from cameras at different locations, a Dual Photometric Stereo process [**Ikeuchi 87**] has been implemented for the recovery of a depth map from the photometric-disparity fields. An interesting feature of such process is that both the matching of the photometric stereo images and the subsequent matching of the disparity maps thus obtained can be performed with a single correspondence algorithm; for instance, with the stochastic matching approach of [**Barnard 86**], or with the neural net implemantation which we have employed here.

References

[**Barnard 82**] Barnard, S.T., and M.A. Fischler, *Computational Stereo*, Computing Surveys, vol. 14(4), pp. 553–572, 1982.

[**Barnard 86**] Barnard, S.T., *A Stochastic Approach to Stereo Vision*, in Procs. 5th National Conf. on AI, USA, pp. 676-680, 1986.

[**Grimson 86**] Grimson, W.E.L., *From Images to Surfaces*, The MIT Press, Cambridge, MA, 1986.

[**Horn 77**] Horn, B.K.P., *Understanding Image Intensities*, Artificial Intell., vol. 8(11), pp. 201–231, 1977.

[**Horn 84**] Horn, B.K.P., *Extended Gaussian Images*, Procs. IEEE, vol. 72, pp. 1671–1686, 1984.

[**Horn 86**] Horn, B.K.P., *Robot Vision*, The MIT Press, Cambridge, MA, 1986.

[**Ikeuchi 87**] Ikeuchi, K., *Determining a Depth Map Using a Dual Photometric Stereo*, Int. J. Robotics Research, vol. 6(1), 1987.

[**Kirkpatrick 83**] Kirkpatrick S., C.D. Gelatt, Jr., and M.P. Vecchi, *Optimization by Simulated Annealing*, Science, 220(4598), pp. 671–680, 1983.

[**Torreão 92**] Torreão, J.R.A., and C.J.L. Pimentel *Disparity-Based Photometric Stereo*, in Procs.l8th Latin-American Informatics Conference, PANEL 92, Spain, pp. 1166–1181, 1992.

[**Torreão 93**] Torreão, J.R.A., and C.J.L. Pimentel *Obtaining Intrinsic Shape Properties with a Disparity Based Photometric Stereo*, submitted to the 19th. Latin-American Informatics Conference.

[**Weinshall 91**] Weinshall, D., *Direct Computation of Qualitative 3-D Shape and Motion Invariants*, IEEE Trans. PAMI, vol. 13(12), pp. 1236-1240, 1991.

[**Woodham 80**] Woodham, R.J., *Photometric Method for Determining Surface Orientation from Multiple Images*, Optical Engineering, vol.19(1), pp.139-144, 1980.

[**Woodham 88**] Woodham, R.J., *Stable Representation of Shape*, in "Computational Processes in Human Vision: An Interdisciplinary Perspective", Z. Pylyshyn (ed.), pp. 443–461, Ablex Publishing Corp., 1988.

[**Woodham 89**] Woodham, R.J., *Determining Surface Curvature with Photometric Stereo*, in Procs. IEEE CVIP Conference, USA, pp. 36–42, 1989.

[**Zhou 88**] Zhou, Y.T., and R. Chellappa, *Stereo Matching Using a Neural Network*, Procs. of the IEEE ASSP Conference, pp. 940–943, New York, 1988.

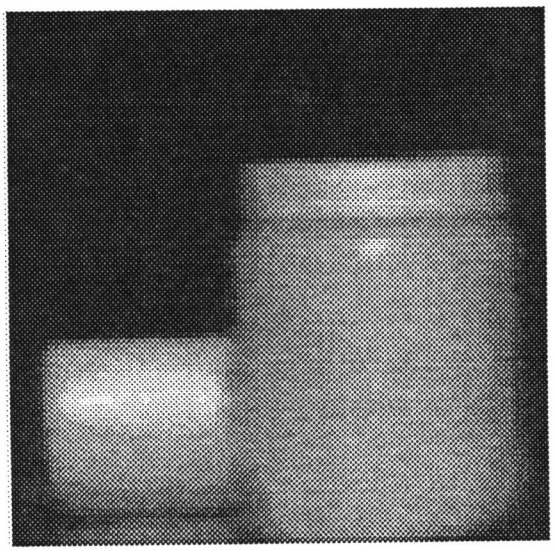

Figure 1a

Figure 1b

Figure 1c

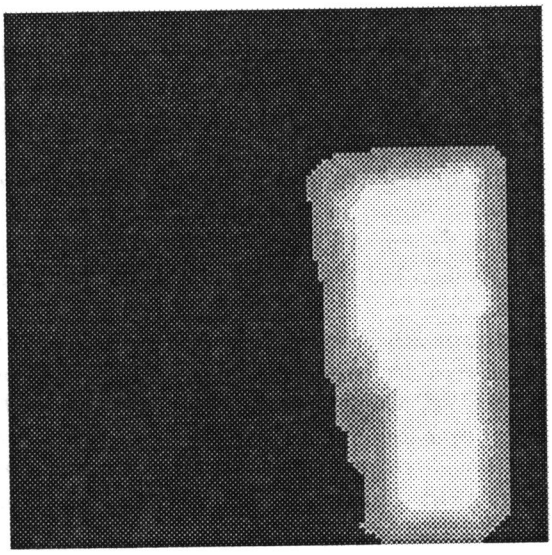

Figure 1d

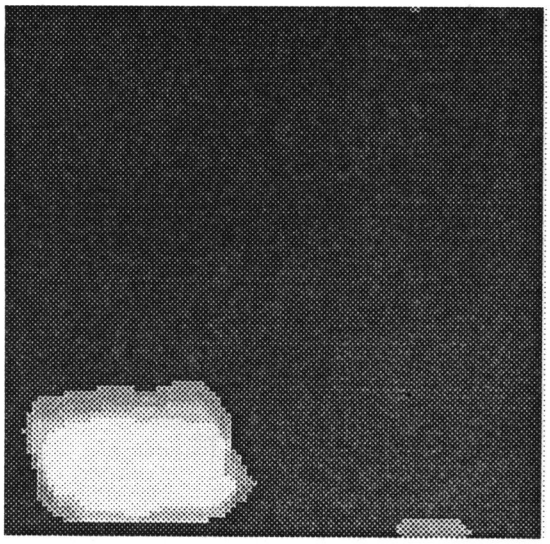

Figure 1e

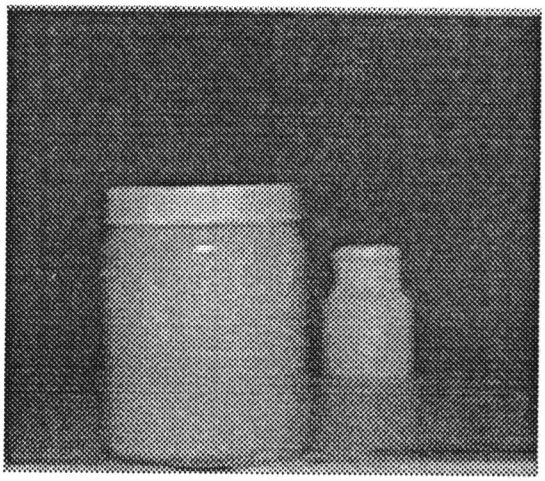

Figure 2a

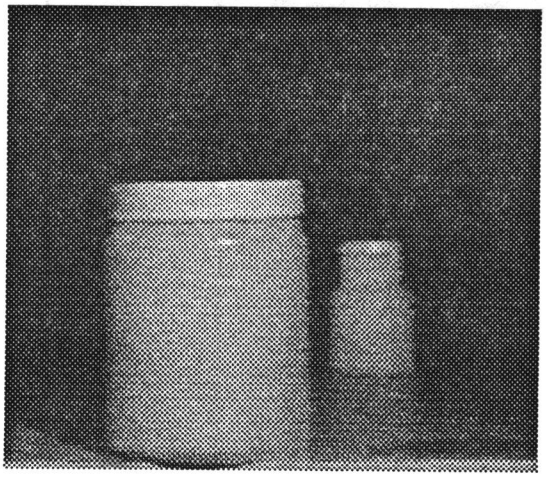

Figure 2b

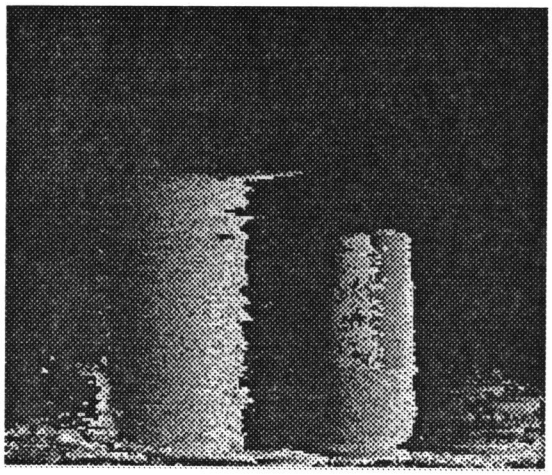

Figure 2c

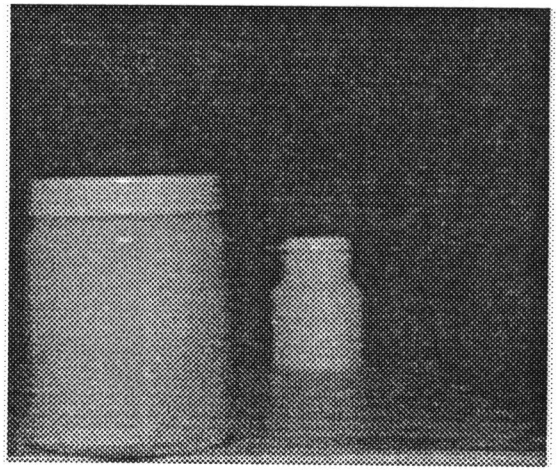

Figure 2d

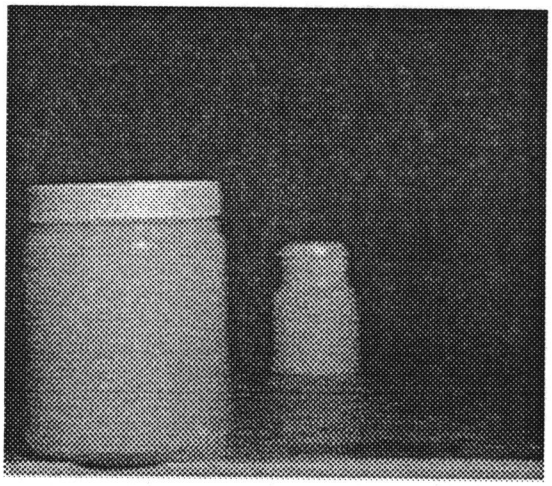

Figure 2e

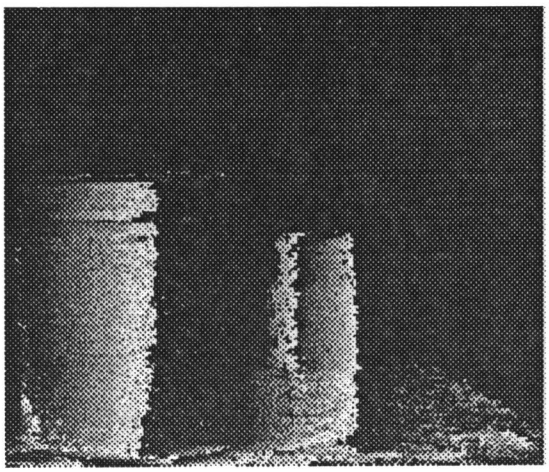

Figure 2f

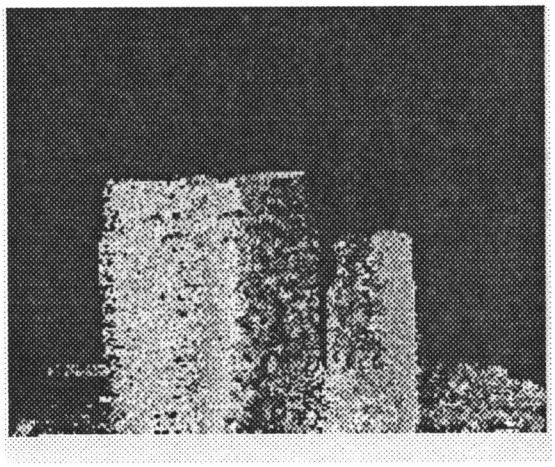

Figure 2g

Figure 3a

Figure 3b

Figure 3c